ELSEVIER

Polymer 43 (2002) 1331–1341

polymer

www.elsevier.com/locate/polymer

Effect of blend ratio on bulk properties and matrix–fibril morphology of polypropylene/nylon 6 polyblend fibers

Mehdi Afshari[a], Richard Kotek[b,*], Mohammad Haghighat Kish[a], Hosein Nazock Dast[c], Bhupender S. Gupta[b]

[a]*Department of Textile Engineering, Amir Kabir University of Technology, P.O. Box 15875-4413, Tehran, Iran*
[b]*College of Textiles, Textile Engineering Chemistry and Science, North Carolina State University, P.O. Box 8301, Raleigh, NC 27695-8301, USA*
[c]*Department of Polymer Engineering, Amir Kabir University of Technology, P.O. Box 15875-4413, Tehran, Iran*

Received 24 July 2001; received in revised form 3 October 2001; accepted 5 October 2001

Abstract

Ternary blends of polypropylene (PP), nylon 6 (N6) and polypropylene grafted with maleic anhydride (PP/N6/PP-*g*-MAH) as compatibilizer with up to 50 wt% of N6 were investigated. PP-*g*-MAH content was varied from 2.5 to 10%. Blends of the two polymers PP/N6 (80/20) without the compatibilizer were also prepared using an internal batch mixer and studied. The ternary blends showed different rheological properties at low and high shear rates. The difference depended on the amount of N6 dispersed phase. Co-continuous morphology was observed for the blend containing 50% N6. This blend also exhibited higher viscosity at low shear rate and lower viscosity at high shear rates than the value calculated by the simple rule of mixture. At higher shear rates, viscosity was lower than that given by the rule of mixture for all blend ratios. An increase in viscosity was observed in the 80/20 PP/N6 blend after the concentration of the interfacial agent (PP-*g*-MAH) was increased. Polyblends containing up to 30% N6 could be successfully melt spun into fibers. DSC results showed that dispersed and matrix phases in the fiber maintained crystallinity comparable to or better than the corresponding values found in the neat fibers. The dispersed phase was found to contain fibrils. By using SEM and LSCM analyses we were able to show that the N6 droplets coalesced during melt spinning which led to the development of fibrillar morphology.

Keywords: Matrix–fibril morphology; Polypropylene; Nylon 6

1. Introduction

Blending immiscible polymers is widely considered as a viable and economical technique for producing polymeric products that have a desirable combination of properties and have the ability to be recycled after the initial product has served its purpose [1–4]. When blended together, most resultant polymers exhibit a two-phase morphology—the major component forms a matrix and the minor appears as the dispersed phase in the form of spheres, platelets or fibrils. In some cases, an interpenetrating network is obtained [5,6]. The factors determining the morphology of an immiscible blend are blending history, blend ratio, interfacial tension, differences in viscosity and elasticity of the two polymers and processing conditions, i.e. temperature, residence time, shear rate, shear stress and total strain [7–20].

Blends of polyamides and polyolefins are of particular interest. Blending of polypropylene (PP) and nylon 6 (N6) can lead to materials with improved chemical and moisture properties, dimensional stability, thermo-mechanical characteristics, impact resistance, flexural modulus, and oxygen permeation. Resulting materials can be produced into products with greater ease and at reduced cost [21,22]. However, to achieve such end results from a polypropylene/polyamide blend, some form of compatibilization is generally required; one successful approach has been the addition of polypropylene grafted with maleic anhydride (PP-*g*-MAH) as a third component [21,23–28]. The maleic anhydride (MAH) units react with the amine end groups of N6 to form block or graft copolymers that act as a compatibilizer for the blend [29].

During the last two decades, the formation of polymer blends that result in a fibrillar phase morphology (FPM) has been extensively investigated. The focus has been on understanding the principles that lead to the formation of such morphology [27]. It has been found that among fiber

* Corresponding author. Tel.: +1-919-515-6585; fax: +1-919-515-6532.
E-mail address: rkotek@unity.ncsu.edu (R. Kotek).

0032-3861/02/$ - see front matter
PII: S0032-3861(01)00689-9

spinning, extrusion and injection molding, fiber spinning is the most conducive method to create this morphology because the elongational force field existing in the spinning process is more effective in producing the fibrillar morphology than the shear force field existing in the other two processes [30].

Several papers have been published on fibers made from blends of polymers [30–34], most particularly fibers from blends of PP and N6 [35–41]. Takahashi [35–37] studied the physical properties of PP/N6 fibers. Grof [39] investigated the structure–property relationship in modified polypropylene–polycaproamide fibers containing MAH grafted PP. Lyoo [34] used blends containing modified PET and PP for producing microfibers by extracting continuous phase. Microfibers obtained after extraction of the continuous phase from an immiscible blend have proven useful for making artificial leather for apparel and other textile products with novel properties. However, little information is available in scientific literature that sheds light on the differences that exist in the morphologies of the polyblend material prior to and after extrusion into fibers. To translate optimally the properties of individual components into that of the polyblend fiber such understanding is essential.

In the present study, the structure and properties of both the polyblends and the polyblend fibers were examined. For the first part, two sets of samples were produced and characterized for morphological properties. In the first set, the effect of blend ratio of PP and N6 was studied in the presence of a constant amount of PP-*g*-MAH. In the second set, a single PP/N6 composition 80/20 was used, and the effect of the amount of PP-*g*-MAH was examined. Rheological, thermal and morphological properties were evaluated. For the second part, polyblends were extruded into fibers using melt-spinning equipment. The fibers so obtained were examined for morphology with a scanning electron microscope (SEM) and a laser scanning confocal microscope (LSCM). Thermal properties were examined with a differential scanning calorimeter (DSC), and the crystal size was determined with a wide angle X-ray diffraction instrument (WXRD).

2. Experimental

2.1. Materials

Commercial fiber grade isotactic PP, known as V30S, was obtained from Arak Petrochemical Co., Iran. PP had a melt flow index (MFI) of 16 g/10 min, density of 0.92 g/cm^3 and T_m of 166 °C. Fiber grade N6 was obtained from Parsilon Co., Iran. N6 had MFI of 26 g/10 min, density of 1.14 g/cm^3 and T_m of 218 °C. PP-*g*-MAH (trade name PB 3150) was received from Uniroyal Chemical Co., USA. This polymer had a MFI of 50 g/10 min, MAH index of 1.5% and density of 0.9 g/cm^3. PB 3150 was used as the compatibilizer for the preparation of the PP/N6 blends. Irganox B215 (Ciba-Geigy, USA) was used as an antioxidant at 0.1 wt% for the preparation of all polyblends.

2.2. Preparation of polyblend polymers

N6 was dried in vacuum oven for 24 h at 80 °C. Polymer blends were prepared by melt mixing in a Haake Rheocord 90 internal batch mixer at 230 °C with a rotor speed of 60 rpm. Blending was carried out by first feeding PP and Irganox B215 into the mixer. After mixing for 2 min, N6 was charged and blending was continued for an additional 3 min. Finally, PP-*g*-MAH was added into the mixer and mixing was carried on for an additional 2 min. The mixture was then extruded and pressed between two metal plates and cooled to the ambient temperature. These blends were ground using a laboratory grinding mill. The blend compositions are given in Table 1. Three sets of samples can be identified:

1. A1, A2 and A7 comprise the set of samples that contains no compatibilizer. A1 is PP, A2 is N6 and A7 is the blend containing 80% PP and 20% N6.
2. A3–A6 comprise the set of samples that contains a constant level of compatibilizer (5%) but varying amounts of PP and N6.
3. A4, A7–A9 comprise the set in which the fraction of N6 was maintained constant at 20%, the amount of compatibilizer was varied from 0 to 10%, and the amount of PP was varied from 80 to 70% to make up the 100% composition.

2.3. Melt spinning of polyblends into fibers

Before melt spinning, the polymer blends were dried in a vacuum oven for 24 h at 80 °C. Melt spinning was performed on a single-screw ($L/D = 26$) Brabender melt extruder with a spinneret containing 20 orifices, each of 1 mm diameter. The extruder was set with five different temperature zones, 200, 210, 230, 240, and 250 °C, respectively, at the feed, metering, die and spinneret sections. The screw was run at 15 rpm. Undrawn filaments were collected at a take-up speed of 50 m/min.

Table 1
Blend compositions

Sample code	PP (wt%)	N6 (wt%)	PP-*g*-MAH (wt%)
A1	100	0	0
A2	0	100	0
A3	85	10	5
A4	75	20	5
A5	65	30	5
A6	45	50	5
A7	80	20	0
A8	77.5	20	2.5
A9	70	20	10

2.4. Rheological measurements

Apparent melt viscosity was determined on an Instron Model 3211 capillary rheometer. The round die used had a length/diameter ratio of 40 and an entrance angle of 90°. Barrel temperature was kept at 230 °C. Plunger speeds were 20, 6, 2, 0.6, 0.2 and 0.06 cm/min. Calculated shear rates varied from 10 to 10,000 s^{-1}. Shear stress was calculated with Eq. (1):

$$\tau_w = \frac{\Delta p}{2L/R} \tag{1}$$

where, Δp is the pressure change, L is the length of the capillary and R is the radius of the capillary.

A modified Metzner form of Rabinowitsch's equation (Eq. (2)) was used for calculating the shear rate

$$\dot{\gamma}_w = 275.568 \frac{3n' + 1}{4n'} \nu \tag{2}$$

where, ν is the speed of the plunger, $n' = \mathrm{d} \ln \tau_w / \mathrm{d} \ln \dot{\gamma}_{w,a}$ and $\dot{\gamma}_{w,a}$ is the shear rate at the wall, τ_w is the shear stress at the wall.

2.5. Scanning electron microscopy

Morphology of the polyblends was studied with a scanning electron microscope (SEM S360, Cambridge Instruments). SEM micrographs were taken from cryogenically fractured surfaces of polyblend specimens after submersion in liquid nitrogen for 1 h. In order to remove the N6 disperse phase, the fractured surfaces of the PP/N6 polyblends were etched for 24 h at room temperature with 98% (by weight) formic acid solution. The surface was then sputter coated with a layer of gold–palladium before viewing.

It was of interest to examine the morphology of the N6 fibrils found in the polyblend fibers. This was accomplished by extracting the PP matrix with decahydronaphtaline (decalin). A 98% formic acid solution was also used to dissolve the N6 phase from the whole fibers, which allowed us to determine the nature of the distribution of N6 fibrils in the cross-section of the polyblend fibers.

2.6. Laser scanning confocal microscopy

LSCM is a non-destructive powerful tool for reconstructing and examining local three-dimensional structures with a high degree of accuracy [42]. Using this technique on a two-phase polymeric material has the added advantage that the light beam can interact with the two phases differentially. This allows an effective means for examining and characterizing in situ the phase distribution and separation phenomena in polyblend materials [42]. The microscope can be used to construct images in various scanning modes, including planar section (*XY* scan), vertical section (*XZ* scan), and time dependent programmed scan.

Only limited work involving the use of LSCM on fibers has appeared in scientific literature [43]. To our knowledge, the matrix–fibril morphology of polyblend fibers has not been studied using this technique.

The fibers were dyed with 0.1 g/l flourescein (C. I. Acid Yellow 73) at pH 6, in an infinite dye bath at 95 °C for 60 min. Dyeing of the fibers was carried out in Ahiba Texomat GVIIB dyeing equipment. N6 fibrils in the polyblend fibers are expected to absorb flourescein dye and, therefore, provide contrast between the two phases, i.e. the PP matrix and the N6 fibril. The fibers were viewed using a Leica DMRBE LSCM which was equipped with three laser systems: an Ar-ion (488 and 514 nm), Kr-ion (568 nm) and He–Ne (632.8 nm). For the purpose of imaging, the 488 nm line of the Ar-ion laser was used with a 40X, 1.25 NA, oil immersion objective.

2.7. Differential scanning calorimetry

A Perkin–Elmer differential scanning calorimeter (Model DSC7), calibrated with indium, was used to study the thermal behavior of the polyblend fibers. Specimens of 3–5 mg were encapsulated in aluminum pans and heated at a heating rate of 10 °C/min from room temperature to 250 °C, and subsequently cooled to room temperature. The fusion enthalpies $\Delta H_{f,PP}$ and $\Delta H_{f,N6}$ were measured and the degrees of crystallinity $X_{c,PP}$ and $X_{c,N6}$ of PP and N6 phases respectively were calculated from the following equations

$$X_{c,N6} = \frac{\Delta H_{f,N6}}{\Delta H^0_{f,N6}} \frac{1}{w_{N6}} 100\% \tag{3}$$

$$X_{c,PP} = \frac{\Delta H_{f,PP}}{\Delta H^0_{f,PP}} \frac{1}{w_{PP}} 100\% \tag{4}$$

where, $\Delta H^0_{f,PP}$ of 50 cal/g and $\Delta H^0_{f,N6}$ of 55 cal/g are the fusion enthalpies of completely crystalline PP and N6 materials [21], respectively, and w_{PP} and w_{N6} are the weight fractions of PP and N6 in the polyblend fibers.

2.8. X-ray analysis of polyblend fibers

A Siemens X-ray diffraction unit operated at 30 kV and 20 mA, with Cu element and nickel filter was used to measure the crystal size of polyblend fibers. The radiation utilized was Cu Kα with a wavelength of 1.54 Å. Fibers were hand wound on a sample holder; the latter was positioned perpendicularly to the X-ray beam. Crystal size was calculated from the Scherrer's equation [44]

$$L = \frac{0.9\lambda}{\beta \cos \theta} \tag{5}$$

where, L is the crystallite dimension, λ is the wavelength, β is the breadth at half maximum intensity, and θ is the Bragg angle.

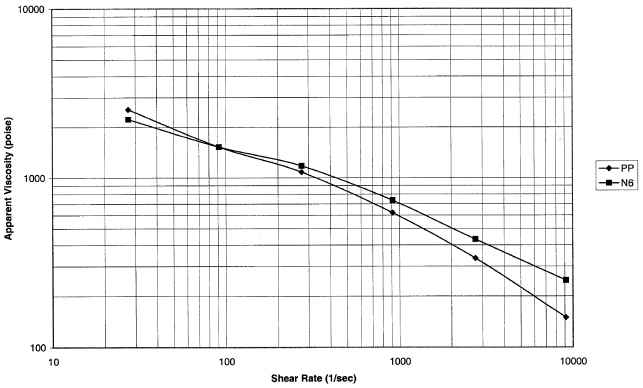

Fig. 1. Apparent melt viscosity of PP and N6 polymers at 230 °C.

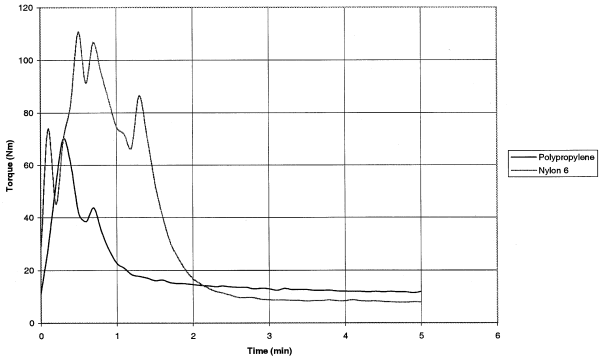

Fig. 2. Torque as a function of mixing time for PP and N6 at a rotor speed of 60 rpm.

3. Results and discussion

3.1. Rheological properties of polyblends

The molecular weights of PP and N6 significantly differ from each other, and therefore one of the problems faced was to determine the range of temperatures at which the blends could be effectively processed. The range of 260–275 °C is usually suited for processing N6, but was not acceptable for PP because of the potential for degradation of PP. We found that processing the blend at a relatively lower temperature, such as 230 °C, resulted in small viscosity divergence, as shown in Fig. 1. The plots reveal, interestingly, that the apparent viscosity exhibits the power law behavior given by Eq. (6)

$$\eta = K\dot{\gamma}^{n-1} \tag{6}$$

where K is consistency and n represents the flow index.

We fitted our data to Eq. (6) and determined the value of the flow index. The correlation coefficient was 0.98. At high shear rates, shear-thinning behavior was more noticeable for PP than for N6. The values of n, the flow index, obtained were 0.623 and 0.523, respectively, for N6 and PP. At a low shear rate ($\sim$100 s^{-1}), the viscosities of PP and N6 are about the same.

Fig. 2 shows a typical curve of torque versus time for a rotor speed of 60 rpm at 230 °C. At this speed, the difference in the viscosities of PP and N6 is lower than the difference in viscosities at 30 and 45 rpm. Wu [10] has indicated that very small polymer droplets are generated when the viscosity ratio, η_d/η_m, of the dispersed phase to the matrix, is near unity. The viscosity difference was found to be higher for the rotor speeds of 30 and 45 rpm.

The rheological properties of polyblends are associated with the phase morphology. Figs. 3a and b shows viscosity as a function of composition at three different shear rates. At the shear rate of 10 s^{-1}, appreciable negative and positive deviations are noted from the value given by the simple additive rule of viscosity mixtures (Eq. (7))

$$\eta = w_{PP}\eta_{PP} + w_{N6}\eta_{N6} \tag{7}$$

where η, η_{PP} and η_{N6} are the apparent viscosities for the polymer blend, PP and N6, respectively, and w_{PP} and w_{N6} are the respective weight fractions of the two components.

Positive deviation generally occurs either when there are strong interactions among droplets or when the blends have an interlocked morphology. It is speculated that when the amount of N6 in the blend is over 30%, the morphology of the blend corresponds to a sea and island or a co-continuous arrangement. At higher shear rates, i.e. 1000 and 10,000 s^{-1}, the blend compositions show negative viscosity deviation (Fig. 3b). Negative viscosity deviation for immiscible polymer blends is associated with an increase in specific volume and voids at the interfaces [45,46]. At higher shear rates, the particles of dispersed phase become finer. Park et al. [26],

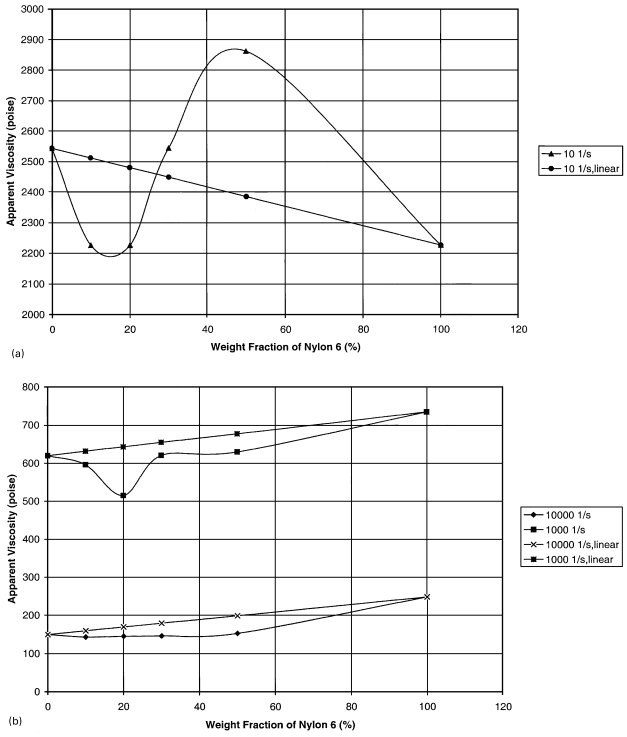

Fig. 3. Apparent viscosity of blends as a function of wt% fraction of N6 (a) at a shear rate of 10 s^{-1}, (b) at shear rates of 1000 and 10 000 s^{-1}.

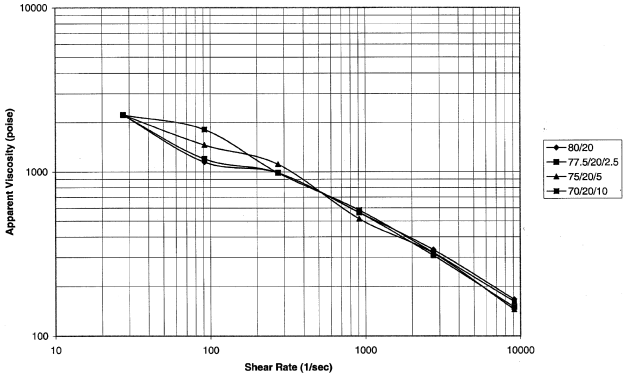

Fig. 4. Apparent viscosity of 80/20 polyblend versus shear rate at different amounts of PP-*g*-MAH.

Hietaoja et al. [47], and Utracki et al. [12] have reported similar results for viscosity-composition dependencies of PP/N6 blends, N66/PP blends and HDPE/N6 blends, respectively.

Fig. 4 shows the effect of shear rate on melt viscosity for the 80/20 (PP/N6) blend at different levels of PP-*g*-MAH. With an increase in shear rate, the apparent viscosity decreased for all blends as expected. However, with an increase in the amount of PP-*g*-MAH in the blend, an increase in viscosity is noted. This increase in viscosity is most likely due to a decrease in the mobility of chains at the interface caused by a chemical reaction between the amine end group of N6 and the MAH group of PP-*g*-MAH. This reaction illustrates that PP-*g*-MAH is performing its function as a compatibilizer [48]. Similar behavior has been reported by Zhang et al. [49] for N10,10/PP blends. Because the compatibilizer establishes strong interaction between the two phases, it is expected that a high shear force would be required to deform the N6 droplets. This also means that large differences in viscosities at low shear rates and small difference in viscosities at high shear rates will be expected among materials containing different amounts of PP-*g*-MAH, as noted in the present results. Intermolecular forces are able to resist deformation at low shear rates, but are disrupted at higher shear rates, as suggested by Heikens et al. [50] and Berger et al. [13].

3.2. Morphology of fractured surfaces of polyblends

The results obtained from the morphological studies of

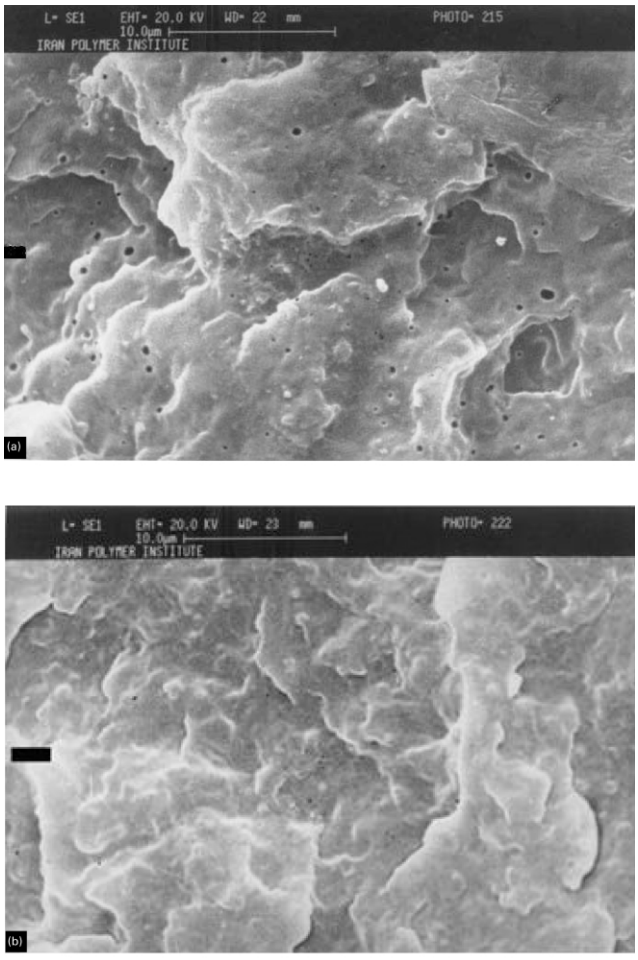

Fig. 5. SEM micrographs of cryogenically fractured surface of (a) 85/10/5 polyblend, (b) 45/50/5 polyblend after etching with 98% formic acid.

cryogenically fractured surfaces, treated with 98% formic acid, are shown in Fig. 5a. It is seen from the data given in Table 2 that as the amount of N6 in blends increased, the size of spherical particles also increased as expected. From the theoretical point of view, an increase in the amount of dispersed N6 should result in an increase in the particle size of this phase. This should be further aided by the fact that at low shear rates, N6 droplets would be subjected to small deformation, the latter determining the droplet size and interactions between the phases. Therefore the 45/50/5 (PP/N6/PP-*g*-MAH) blend showed (Fig. 3a) higher viscosity than the simple rule of mixture at the shear rate of 10 s^{-1}.

Table 2
Size of spherical dispersed N6 particles in polyblend before producing fibers and calculated N6 fibril lengths in polybend fiber (d_n and d_w are the number and weight average particle diameter)

Sample code	Particle diameter d_n (μm)	Particle diameter d_w (μm)	d_w/d_n	Fibril diameter d_f (μm)	Calculated fibril length L_c (μm)
A3 (85/10/5[a])	0.3 ± 0.1	0.33	1.1	0.14 ± 0.04	0.92
A4 (75/20/5)	0.32 ± 0.09	0.35	1.09	0.23 ± 0.1	0.41
A5 (65/30/5)	0.47 ± 0.2	0.58	1.23	0.27 ± 0.1	1.78
A7 (80/20)	2.74 ± 0.52	2.9	1.06	1.04 ± 0.6	3.42

[a] PP/N6/PP-*g*-MAH.

The blend of 45/50/5 (PP/N6/PP-*g*-MAH) can be described as one supporting the sea and island or co-continuous morphology (Fig. 5b). Since, it was difficult to determine the locations of the PP or N6 phases in this blend, we used the model of Jordhamo et al. [6], given below, to determine whether phase-inversion occurred at low shear rates

$$\frac{\eta_m}{\eta_d}\frac{\phi_d}{\phi_m} = 1 \tag{8}$$

The quantities η_m and η_d represent the viscosities of the matrix and the dispersed phase, respectively, whereas ϕ_m and ϕ_d represent the respective volume fractions of the two phases. At $\dot{\gamma} = 27\ s^{-1}$, the corresponding viscosities found were 2543.872 poise for PP and 2225.984 poise for N6. This gave $\eta_m/\eta_d = 1.143$. Since $\phi_d/\phi_m = 0.877$, $(\eta_m/\eta_d)(\phi_d/\phi_m = 1.002)$. Such excellent agreement with the Joradhamo model allowed us to conclude that the phase-inversion occurred in the 45/50/5 blend at this low shear rate.

At a high shear rate of $\dot{\gamma} = 912.8\ s^{-1}$, $(\eta_m/\eta_d)(\phi_d/\phi_m = 0.74)$. This value is far from 1, and indicates that phase inversion didn't occur in the 45/50/5 blend at this shear rate. The Jordhamo model becomes weak and less applicable at the high shear rate, in agreement with the findings of some previous investigators [47].

In order to measure the diameter and length of fibrils of the dispersed phase, SEM pictures prepared after etching N6 or extracting PP were scanned and evaluated with an image analysis system. The diameters of droplets and fibrils of the dispersed phase were determined. N6 particle size found in the 75/20/5 compatibilized blend was 0.32 ± 0.09 μm while that found in the 80/20 noncompatibilized blend was 2.74 ± 0.52 μm.

SEM micrographs Fig. 6a and b and data in Table 2 show a large decrease in N6 particle size after the addition of the compatibilizer. The addition of 5 wt% PP-*g*-MAH to the 80/20 blend greatly reduced the average N6 particle size, i.e. from 2.74 to 0.32 μm. The phase morphology of the non-compatibilized 80/20 blend is poor and the dispersed N6 particles are large, owing to the inherent immiscibility of N6 with PP. Increasing the compatibilizer content beyond 5 wt% had little further effect on the particle size of the dispersed phase. Duvall [51] showed that the particle size correlated better with the concentration of anhydride groups in the blend, rather than with the amount of compatibilizer. Miettinen [48], working on N6/PP polyblends, showed that the difference in morphologies obtained with 5 and 10 wt% compatibilizer (SEBS-*g*-MAH) was not significant. (SEBS stands for styrene–ethylene–butylene–styrene block copolymer.)

The morphology of compatibilized blends appeared highly homogeneous (Fig. 6a), indicating the presence of strong interaction and adhesion between the PP and N6 phases. This was most probably due to the formation of a PP-*g*-MAH/N6 copolymer by the reaction of anhydride groups with terminal amide groups of N6 during melt mixing. The compatibilized blends exhibited much finer dispersed phases than did the non-compatibilized blend. Homogeneity and the decreased size of the dispersed phase in compatibilized blends apparently also led to an increase in the surface area of the dispersed phase in contact with the matrix, which further resulted in better adhesion between the two.

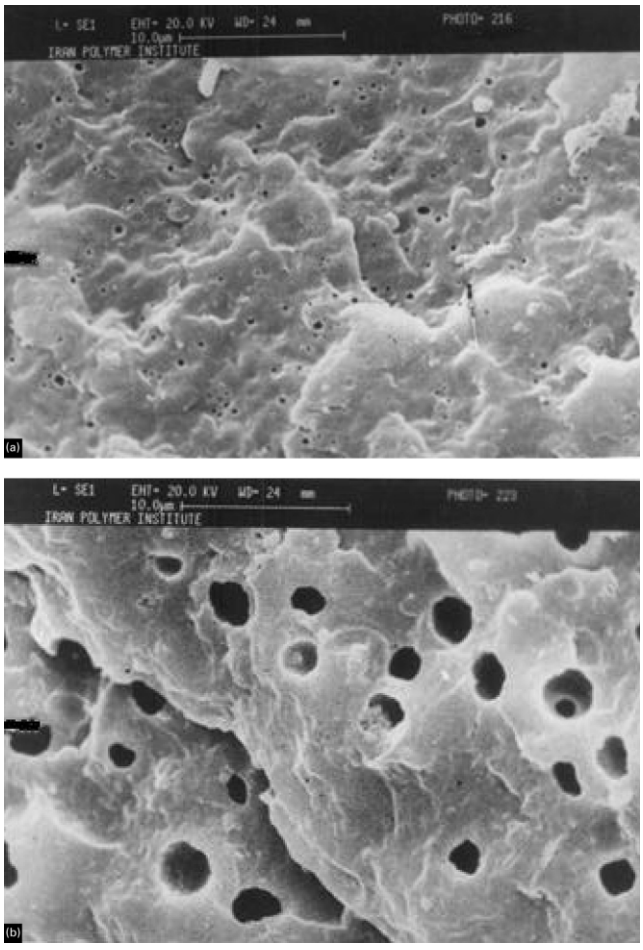

Fig. 6. SEM micrographs of cryogenically fractured surface acid of (a) 70/20/10 polyblend after etching with 98% formic acid, (b) 80/20 polyblend without etching.

3.3. Spinnability of polyblend into fibers

Typical spinning conditions used have been mentioned in Section 2.3. However, it was found necessary to sometimes adjust the conditions somewhat to obtain optimum results. We were able to successfully make undrawn fibers from polyblends containing up to 30 wt% of N6. Unstable conditions were encountered during the spinning of blends containing a higher fraction of nylon, i.e. 45/50/5 composition. Consequently, we could not produce fiber from that blend. It could be that a greatly decreased viscosity or increased particle size of N6 was responsible for such a behavior. The polyblend fibers were mechanically robust. They had elongation in the range from 430 to 600%. After drawing three times, tenacity was in the range 3.3–5.0 g/d.

Table 3
DSC thermal properties and percent crystallinity for PP, N6 and polyblend fibers

Sample code	T_m of PP (°C)	T_m of N6 (°C)	% crystallinity of PP in fiber	% crystallinity of N6 in fiber	% total crystallinity of fiber[a]
A1 (PP)	164.66	–	37.03	–	37.03
A2 (N6)	–	218.833	–	19.85	19.85
A3 (85/10/5[b])	163.66	218.33	34.11	27.98	31.79
A4 (75/20/5)	163.33	215.33	37.97	24.87	33.45
A5 (65/30/5)	163.83	218.5	39.97	26.57	33.95
A7 (80/20)	163.33	213.66	36.62	27.12	34.72
A8 (77.5/20/2.5)	163.66	213.83	38.56	25.63	35.01
A9 (70/20/10)	164	217.83	41.68	25.89	34.35

[a] Calculated from Eq. (9) for samples A3–A9.
[b] PP/N6/PP-*g*-MAH.

A full evaluation of fiber mechanical properties will be given in the next paper.

Fibers so obtained were etched with formic acid or decahydronaphtaline and examined for blend morphology.

3.4. Thermal analysis of polyblend fibers

The results of DSC analysis of neat fibers and polyblend fibers are summarized in Table 3. As seen from the DSC results in Fig. 7, PP/N6 polyblend fibers exhibited two distinct melting peaks, the lower obviously corresponding to the melting point of PP whereas the higher corresponding to the melting of N6. Since the neat PP and N6 fibers showed only one melting peak each, the two polymers could in general be considered as immiscible.

The melting temperature (T_m) of PP did not appear to be different in the polyblend fibers in comparison to that of the neat PP fiber. The T_m of N6 in the polyblend fibers, on the other hand, was consistently 3–4 °C lower than the value of the corresponding neat fiber. Probably, the lower T_m of N6 in the polyblend fibers could be a result of the formation of block copolymer between PP-*g*-MAH and N6 [52]. Park et al.'s work in PP/N6 blends also showed that the T_m of PP was constant but that of N6 decreased 3–4 °C with an increase in the amount of PP-*g*-MAH [26]. However, Varga [27] believed that the positions of the melting and crystallization peaks attributed to the individual components were practically independent of the composition; only the intensities of the peaks, i.e. the areas under the curves, varied with the ratio of the components. Our results, on the other hand, support the observations of Park et al. in that the positions of the N6 peaks may also shift.

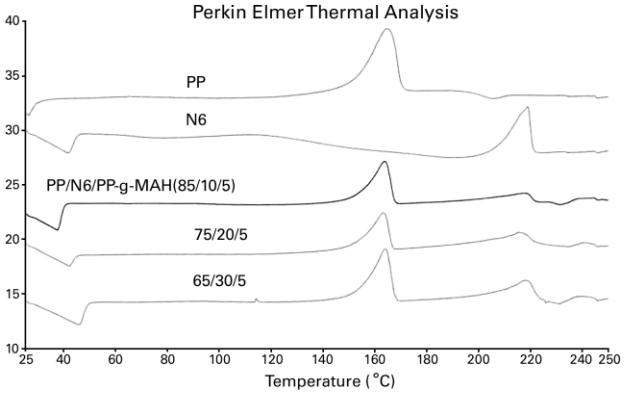

Fig. 7. DSC thermograms of polyblend fibers.

The results of percent crystallinity, assessed from the DSC profiles, are included in Table 3. One of the results noted is that the crystallinity of N6 in the polyblend fibers is higher than the value of the neat fiber. This most likely indicates that PP moieties acted as nucleating agents for N6 in the polyblend fiber. A similar increase in crystallinity did not take place for PP.

We also observed that with an increase in the amount of PP-*g*-MAH in the 80/20 (PP/N6) fiber, the percent crystallinity of PP generally increased and that of N6 generally decreased. Decreasing crystallinity of N6 in the presence of PP-*g*-MAH is a direct consequence of the compatibilization process that is closely related to a higher degree of dispersion for N6 in the PP matrix [53]. Consequently, the formation of the linkage between N6 and PP-*g*-MAH during melt mixing, hindered the packing of polymer chains, resulting in a reduction of the crystallinity of N6 [53,54].

For calculating the total percent crystallinity of polyblend fibers, we assumed that molecular chains of compatibilizer would be more likely in the amorphous regions of both PP and N6. Thus Eq. (9) was used for calculating the total percent crystallinity of polyblend fibers.

$$X_{total} = X_{c,PP} w_{PP} + X_{c,N6} w_{N6} \quad (9)$$

The value of crystallinity of the polyblend fiber is given in the last column of Table 3. The result noted is that the total crystallinity of the polyblend fiber is maintained in spite of the fiber being a composite of two different materials. Accordingly, properties, i.e. physical, mechanical, and chemical, that depends on the degree of crystallinity can be expected to be potentially present in the polyblend fiber. Measurement and examination of these properties in polyblend fibers is the focus of the next paper in this project.

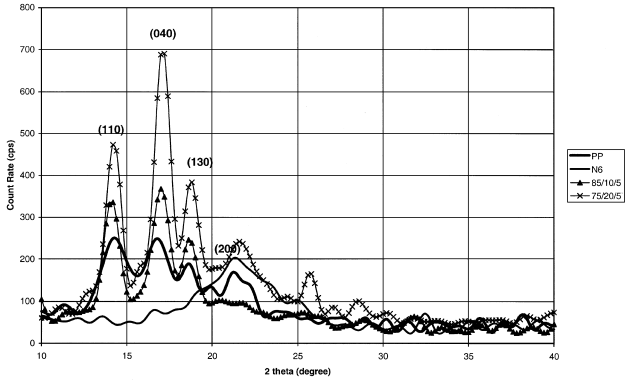

Fig. 8. Wide angle X-ray diffraction spectra of neat PP, N6 and PP/N6 polyblend fibers.

3.5. Wide angle X-ray diffraction analysis of polyblend fibers

The 2θ X-ray diffraction patterns of neat as well as the polyblend fibers are shown in Fig. 8. There were no significant shifts in the diffraction positions of the two materials after forming the polyblend fiber. This shows that the nature of the crystalline lattices of the two materials did not undergo an appreciable change. The intensity of reflections at the angular positions 2θ of 14.2, 16.8 and 18.6°, corresponding, respectively, to the 110, 040 and 130 planes of PP, and 2θ of 21.5° corresponding to the 200 plane of N6, actually increased. This suggests that each polymer component tended to enhance the size and/or perfection of the crystals of the other in the polyblend fiber. Varma and Dhar, while working on N6/PET polyblend fiber, also showed that the lattice planes of N6 were reinforced by PET [55].

Table 4 shows the crystal size of the plane (110) of PP and the plane (200) of N6. The crystal size of both materials in the polyblend fibers is larger than that in the neat fibers. The change in crystal size of PP and N6, noted from the X-ray diffraction data after increase in compatibilizer content, seems to roughly correspond to the change noted in the degree of crystallinity of the two materials assessed from the DSC results. Teli et al. [56] similarly reported an increase in crystal size based on (110) plane of PP material in PP/PBT polyblend fibers.

Table 4
Crystal size of plane (110) of PP and plane (200) of N6 for neat PP, N6 and polyblend fibers

Sample code	D_{110} (Å), PP [40]	D_{200} (Å), N6 [58]
A1 (PP)	50.82	–
A2 (N6)	–	14.47
A3 (85/10/5[a])	107.28	–
A4 (75/20/5)	93.15	24.72
A5 (65/30/5)	83.98	31.09
A7 (80/20)	85.2	19.77
A8 (77.5/20/2.5)	91.67	–
A9 (70/20/10)	138.8	18.37

[a] PP/N6/PP-*g*-MAH.

3.6. Fiber morphology examined under scanning electron microscopy

In order to examine the morphology of polyblend fibers,

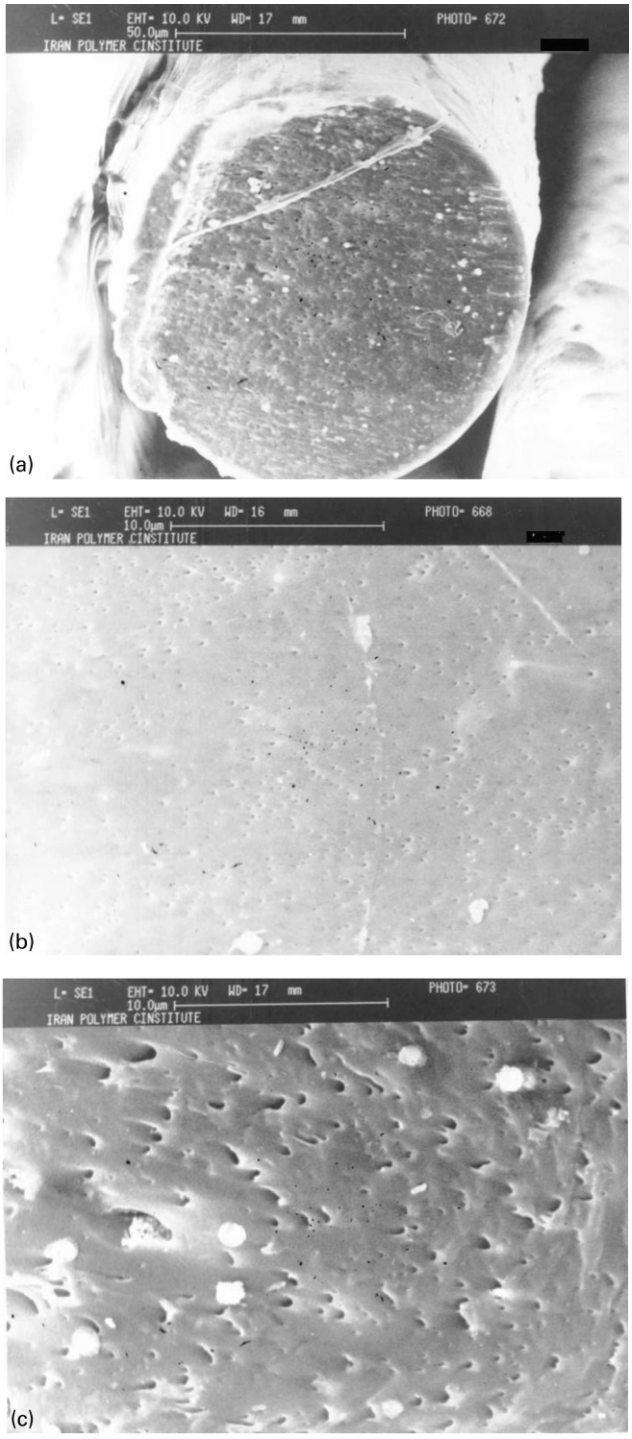

Fig. 9. SEM micrograph of polyblend fiber cross-section of etched (a) 85/10/5 polyblend fiber, (b) 75/20/5 polyblend fiber, (c) 65/30/5 polyblend fiber with 98% formic acid.

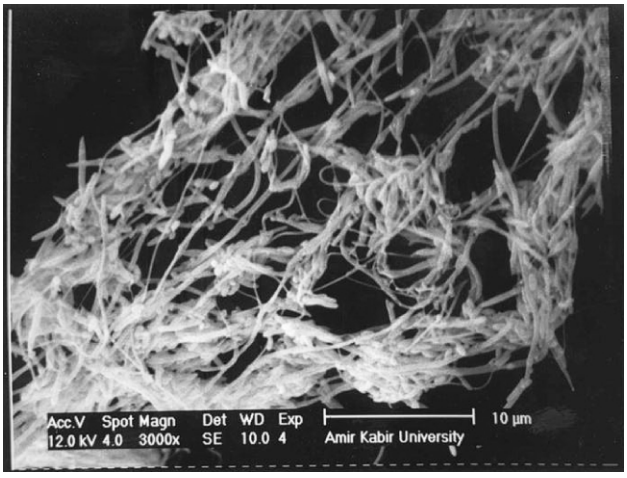

Fig. 10. SEM micrograph of N6 fibrils in 80/20 polyblend fiber after extraction of PP with decahydronaphtaline.

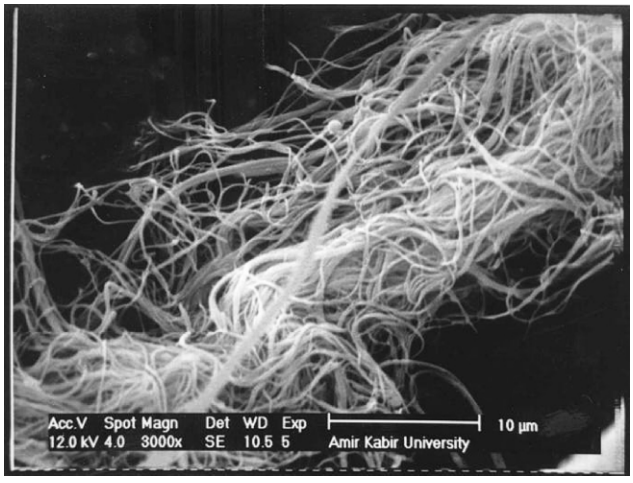

Fig. 11. SEM micrograph of N6 fibrils in 75/20/5 polyblend fiber after extraction of PP with decahydronaphtaline.

we cut the fiber ends with a sharp razor, dipped the ends in 98% formic acid to etch away the N6 fibrils, and observed the morphology from the ends of the fiber. The micrographs in Fig. 9a–c show that the number of fibrils tended to increase with an increase in the fraction of N6 in the fiber. The average diameter of fibrils also appeared to increase with an increase in the amount of N6 (Table 2). The fibrils were found to be located mainly in the core of the filaments and were oriented in the direction of the fiber axis. According to Tsebrenko et al. [57], the fibrils formed in the region where the polymer exited the capillary and they were dispersed uniformly in the cross-section of the fiber.

In order to determine the shape of fibrils in our fibers, the PP matrix was dissolved in decahydronaphtaline. During this treatment, the N6 fibrils remained unchanged. Fig. 10 is a SEM micrograph of the treated 80/20 blend. One sees the N6 polymer but there is little evidence of properly formed fibrils in the structure. This was probably due to the presence of a low degree of interfacial adhesion between the two phases combined with small role elongational forces could play in deforming the N6 droplets during spinning.

Formation of fibrils of N6 was greatly improved when the blends contained the compatibilizer (Figs. 11 and 12). The fibrils formed were also relatively uniform in size. Since it was difficult to determine the length of fibrils directly, we calculated theoretical length, L_c, by assuming that each N6 droplet had converted into a fibril. The average volume, V, of dispersed N6 particles in the polyblends before producing fibers was calculated with Eq. (10)

$$V = \tfrac{4}{3}\pi R_n^3 \tag{10}$$

where R_n is the number average radius of N6 droplets, assuming the latter were essentially spherical. The degree of roundness of the dispersed phase particles, however, was evaluated using Eq. (11). The values of the area A and the perimeter P in the equation were determined by image analysis of the SEM micrographs of the particles. For all polyblends, the value of the degree of roundness was found to lie between 0.85 and 0.9, indicating that the assumption of the particles being spherical in polyblends was reasonable

$$\text{Degree of Roundness} = \frac{4\pi A}{P^2} \tag{11}$$

If each N6 spherical droplet was converted into a fibril, its volume, V, will be given by Eq. (12)

$$V = \pi R_f^2 L_c \tag{12}$$

where R_f is the number average radius of fibril and L_c is the calculated length of the fibril.

Combining Eqs. (10) and (12) we get Eq. (13) for L_c:

$$L_c = \frac{4R_n^3}{3R_f^2} \tag{13}$$

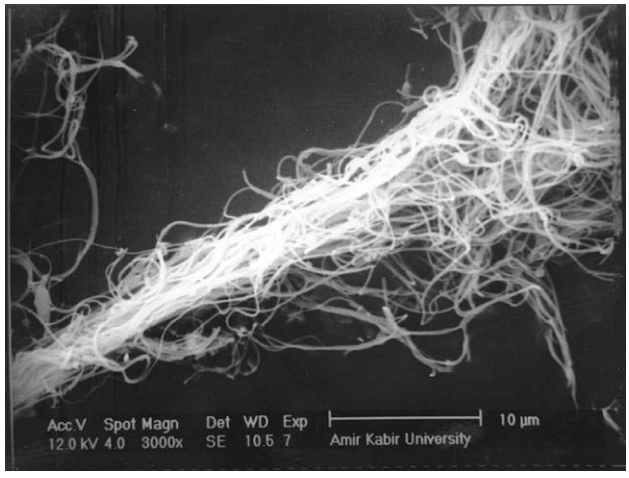

Fig. 12. SEM micrograph of N6 fibrils in 85/10/5 polyblend fiber after extraction of PP with decahydronaphtaline.

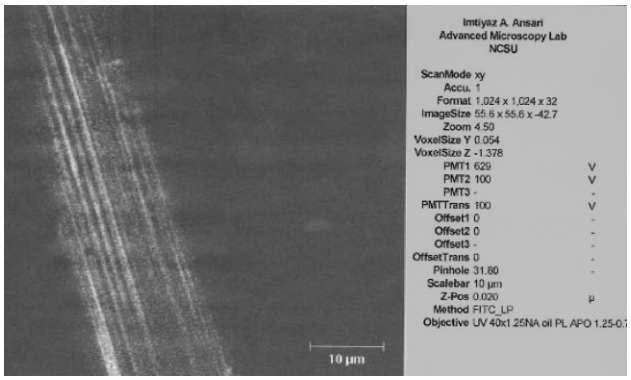

Fig. 13. LSCM image of 65/30/5 polyblend fiber dyed with fluorescein (40X NA 1.25 oil objective).

Calculated values of L_c are given in Table 2 and were found to lie in the range 0.41–3.42 μm. These calculated values of L_c are very low as compared to the measured lengths (Section 3.7), i.e. they are of about the same size as the measured diameters of the fibrils. This suggests that a number of N6 droplets must have coalesced and formed a fibril during melt spinning.

3.7. Fiber morphology determined with laser scanning confocal microscopy

LSCM is a non-destructive and more precise method than SEM for estimating the length of fibrils. After dyeing polyblend fibers with a flourescein dye, we were able to get a contrast between the matrix and the fibrils. We found, however, that we could only observe fibrils that were located near the surface of fibers (Fig. 13). The prolonged exposure of filaments to dye did not improve dye diffusion into the core of the polyblend fibers. Obviously, it would be of great value to be able to come up with a procedure that will allow one to use this non-destructive method for examining the structures that lie in the core of the fiber where, in the present case, more fibrils are located.

The measured length of fibrils varied between 10 and 60 μm as seen from Fig. 13. From SEM micrographs

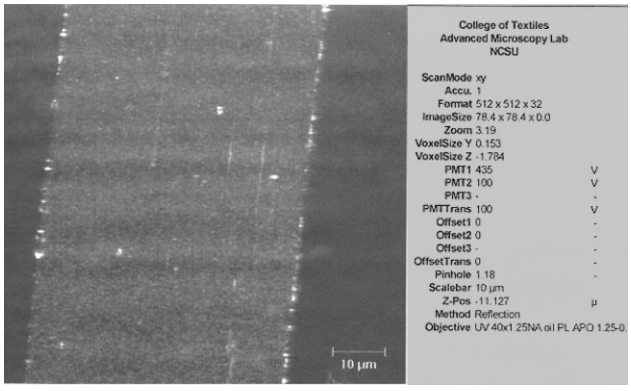

Fig. 14. LSCM image of PP fiber (40X NA 1.25 oil objective).

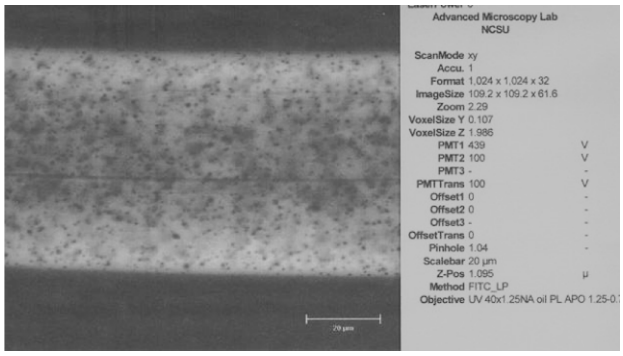

Fig. 15. LSCM image of N6 fiber dyed with flourescein dye (40X NA 1.25 oil objective).

(Figs. 10–12) it is clear that the fibrils are much longer in length (of the order of 10 μm or greater) than the calculated values in Table 2. The difference between the measured and the calculated values confirm that the N6 droplets coalesced during spinning.

It is noted that the hydrophobic PP fiber did not absorb fluorescein at all (Fig. 14), whereas the hydrophilic N6 fiber easily absorbed the acid dye (see Fig. 15). The particles of TiO_2 can also be easily seen in the N6 fiber.

4. Conclusions

Blend composition and interfacial adhesion provided by the compatibilizer were two important factors that influenced the properties of the PP/N6 polyblends. Depending on the fraction of the N6 dispersed phase, the ternary blends showed different rheological properties at low and high shear rates. Generally, an increase in size of dispersed N6 droplets led to a decrease in viscosity greater than that given by the simple additive rule. However, at low shear rates, there were both a decrease and an increase in the viscosity value with an increase in the weight fraction of N6. As we observed, the size of dispersed N6 droplets increased with an increase in the amount of N6 in the polyblends. Sea and islands or co-continuous morphology was assumed to be present in the compatibilized polyblends containing greater than 30% N6 dispersed phase. Accordingly, at low shear rate these blends exhibited positive viscosity departure from the simple additive rule. At higher shear rates, the viscosity departure was negative for all mixing ratios.

It was noted that as the amount of PP-*g*-MAH in 80/20 blends increased, the apparent viscosity at low shear rates increased. Little viscosity difference was observed at higher shear rates, the difference in viscosities of polyblends containing different amounts of PP-*g*-MAH was little.

Polyblend polymers were melt spun into fibers. The DSC results showed that the dispersed and the matrix phases in the fiber maintained crystallinity comparable to or better than the corresponding values found in the neat fibers. The dispersed N6 phase contained fibrils. The latter were

oriented parallel to the axis and distributed throughout the cross-section of the fiber but were more highly concentrated at the center. Theoretical analysis showed that the N6 droplets coalesced together that led to the development of fibrillar morphology.

Acknowledgements

Richard Kotek thanks Mr John Wefer of Uniroyal Chemical Co. for providing a gift of PB 3150. The help of Dr A.R. Oromehie is acknowledged for advising us in the performance of the rheological measurements and providing us the first sample of PP-*g*-MAH. We thank Drs S. Hudson, A. Tonelli and B. Smith for useful comments. Magdalena Kotek is greatly acknowledged for the thorough review of the manuscript.

References

[1] Xanthos M. Polym Engng Sci 1988;28:1392.
[2] Utracki LA. Int Polym Sci Technol 1991;18:38.
[3] Utracki LA. Commercial polymer blends. London: Chapman & Hall, 1998.
[4] Curto D, Valenza A, Lamantia FP. J Appl Polym Sci 1990;39:865.
[5] Vianio TP, Seppala JV. Polym Polym Compos 1993;1:427.
[6] Jordhamo JM, Manson JA, Sperling LH. Polym Engng Sci 1986;26:517.
[7] Van Oene HJ. Colloid Interf Sci 1972;40:448.
[8] Elmendorp JJ, Van Der Vegt AK. Polym Engng Sci 1986;26:1332.
[9] Plochocki AP. Polym Engng Sci 1982;22:1153.
[10] Wu S. Polym Engng Sci 1987;27:335.
[11] White JL, Min K. Adv Polym Technol 1985;5:225.
[12] Utracki LA, Dumoulin MM, Toma P. Polym Engng Sci 1986;26:34.
[13] Berger W, Kammer W, Kummerlowe C. Makromol Chem Suppl 1984;8:101.
[14] Favis BD, Chalifoux JP. Polymer 1988;29:1761.
[15] Plochocki AP, Dagli SS, Andrews RD. Polym Engng Sci 1990;30:741.
[16] Favis BD, Willis JM. J Polym Sci Part B: Polym Phys 1990;28:2259.
[17] Plochocki AP. Polym Engng Sci 1986;26:82.
[18] Favis BD. J Appl Polym Sci 1990;39:285.
[19] Favis BD, Chalifoux JP. Polym Engng Sci 1987;27:1591.
[20] Han CD, Kim YW, Chen SJ. J Appl Polym Sci 1975;19:2831.
[21] Gonzalez-Montiel A, Keskkula H, Paul DR. J Polym Sci Part B: Polym Phys 1995;33:1751.
[22] Utracki LA, Sammut P. Plast Rubber Compos Process Appl 1991;16:221.
[23] Ide F, Hasegawa A. J Appl Polym Sci 1974;18:963.
[24] Van Gheluwe P, Favis BD, Chalifoux JP. J Mater Sci 1988;23:3910.
[25] Scholz P, Frohlich D, Muller R. J Rheol 1989;33:481.
[26] Park SJ, Kim BK, Jeong HM. Int Polym J 1990;26:131.
[27] Varga J, Breining A, Ehrenstein GW. Int Polym Proc 2000;XV:53.
[28] Lee JD, Yang SM. Polym Engng Sci 1995;35:1821.
[29] Macknight WJ, Lenz RW, Musto PV, Somani RJ. Polym Engng Sci 1985;25:124.
[30] Varma DS, Dhar VK. Tex Res J 1988;58:274.
[31] Kiato T, Ashi HK, Ikegami S, Ohya S. J Polym Sci Part A: Polym Chem 1973;11:2633.
[32] Bhat GR, Hersh SP. J Appl Polym Sci, Appl Polym Symp 1977;31:55.
[33] Tsebrenko IA, Pakharenko VA. Fiber Chem 1999;31:23.
[34] Lyoo WS, Choi YG, Ha WS, Kim BC. Int Polym Process 2000;XV:369.
[35] Takahashi T, Konda A, Shimizu Y. Sen-i-Gakkaishi 1996;52:507.
[36] Takahashi T, Konda A, Shimizu Y. Sen-i-Gakkaishi 1994;50:241.
[37] Takahashi T, Konda A, Shimizu Y. Sen-i-Gakkaishi 1996;52:396.
[38] Li X, Chen M, Huang Y. Polym J 1997;29:975.
[39] Grof I, Durcova O, Jambrich M. Colloid Polym Sci 1992;270:22.
[40] Liang BR, White JL, Spruiell JE, Goswami BC. J Appl Polym Sci 1983;28:2011.
[41] Seves A, Testa G, Marcandeli B, Bergamsaco L, Munaretto G, Beltrame PL. Dyes Pigments 1997;35:367.
[42] Ribbe AE. Trends Polym Sci 1997;5:333.
[43] Song Y, Srinivasarao M, Tonelli A, Balik CM, McGregor R. Macromolecules 2000;33:4478.
[44] Alexander LE. X-ray diffraction methods in polymer science. New York: Wiley, 1969.
[45] Chermisinoff NP. Handbook of polymer science and technology. Marcel Dekker: New York, 1989.
[46] Plochocki AP. Polym Engng Sci 1983;23:618.
[47] Hietaoja PT, Holsti-Miettinen RM, Seppala JV, Ikkala OT. J Appl Polym Sci 1994;54:1613.
[48] Holsti-Miettinen R, Seppala J, Ikkala OT. Polym Engng Sci 1992;32:868.
[49] Zhang X, Yin Z, Yin J. J Appl Polym Sci 1996;62:893.
[50] Heikens D, Hoen N, Barensten W, Plet P, Laden H. J Polym Sci, Polym Symp 1978;62:309.
[51] Duvall J, Sellitti C, Myers C, Hiltner A, Baer E. J Appl Polym Sci 1994;52:195.
[52] Li H, Hu GH. J Polym Sci Part B: Polym Phys 2001;39:601.
[53] Beltrame PL, Castelli A, Canauz M, Canetti M, Seves A. Macromol Chem Phys 1995;196:2751.
[54] Beltrame PL, Castelli A, Pasquantonio MD, Canetti M, Seves A. J Appl Polym Sci 1996;60:579.
[55] Varma DS, Dhar VK. J Appl Polym Sci 1987;33:1103.
[56] Teli MD, Ramani VY, Adivarekar RV. J Tex Assoc 1996;56:205.
[57] Tsebrenko MV, Yudin AV, Ablazova TI, Vinogradov GV. Polymer 1976;17:831.
[58] Mishra SP. Asian Tex J 1994;2:62.